# Analysis of STBC-aided energy harvesting cooperative NOMA for Internet of Things

*Olumide Alamu, Thomas O. Olwal and Munguakonkwa Emmanuel Migabo*
Department of Electrical Engineering/F'SATI, Tshwane University of Technology, Pretoria, South Africa

**Abstract**

**Purpose** – This study aims to demonstrate the possibility of integrating a space-time block code (STBC) transmission scheme in a cooperative non-orthogonal multiple access (CNOMA) system with an energy harvesting (EH) relay. Specifically, the authors incorporate the STBC scheme at the source and the relay nodes while considering the existence of direct and indirect paths in the system. This study aims to provide a new approach to augmenting the diversity gain with a guaranteed sustainable network operation of the Internet of Things (IoT) devices, which are designated as the destination nodes in the proposed system.

**Design/methodology/approach** – To examine the effectiveness of the proposed system, the authors adopt a closed-form approach in developing numerical expressions used in gauging the system performance. These include the exact and asymptotic outage probability (OP) analysis, throughput performance, energy efficiency and diversity gain. Further, the authors use MATLAB software to perform the numerical computations.

**Findings** – This study compares the results from the numerical analysis with several benchmark schemes. The results obtained demonstrate the superiority of the solution in comparison to the benchmarks. This is evident from the OP of the destination user equipment, which is improved by approximately 38% and 64% when compared with the conventional EH STBC-aided CNOMA and the case without EH, respectively.

**Originality/value** – This study provides an innovative insight into addressing the foreseeable problem of spectral efficiency, limited data connectivity of IoT devices and energy-constrained operational lifetime of fifth-generation (5G) and beyond 5G networks. Using the STBC transmission scheme and EH in CNOMA systems will support the realization and goals of these communication systems. These goals include seamless connectivity of billions of IoT devices, enhanced achievable data rate and energy-efficient and sustainable network operation.

**Keywords** Cooperative NOMA, Space-time block code, Energy harvesting, Outage probability, Throughput, Energy efficiency

**Paper type** Research paper

## 1. Introduction

For the efficient design of Internet of Things (IoT) systems, the role of radio access technologies that support the seamless and massive connectivity of IoT devices cannot be ignored. Thus, the non-orthogonal multiple access (NOMA) continues to attract research interest in this direction. This technique can employ the power allocation strategy at the source to multiplex several users on the same transmission resources. At the user end, successive interference cancellation (SIC) operation is activated to nullify the unwanted signals from the composite signal (Jorswieck, 2024). Given the significance of the order of user equipment (UE) channel gains in power-domain NOMA (Wei *et al.*, 2024), a near-field UE or dedicated relay node can be used to recreate a line-of-sight path to the destination UE, thus the notion behind cooperative NOMA (CNOMA) (Alamu *et al.*, 2023a; Ashwini and Jagadeesh, 2024; Zeng *et al.*, 2020). Aside from enhancing the spectral efficiency, CNOMA leverages the transmit diversity from the source and relay nodes to provide additional improvement in terms of transmission reliability (Sharma *et al.*, 2024).

Furthermore, owing to the energy limitations of the relays, several studies have demonstrated the possibility of incentivizing the relays by enabling them to glean energy from the radio signals to recharge their batteries. This approach not only sustains the participation of the relays in the cooperative NOMA scheme but also improves the system energy efficiency (Moloudian *et al.*, 2024). An established method of energy harvesting (EH) to accomplish this is simultaneous wireless information and power transfer (SWIPT) (Singh *et al.*, 2024). This method facilitates the concurrent transfer of energy and information in power or time domain (Alamu *et al.*, 2023b; Khalaf *et al.*, 2024).

Recent advances in this direction are presented as follows. In Tran and Vien (2023), the outage probability (OP) and throughput performance of EH receivers operating time switching (TS) and power splitting (PS) protocols are investigated. Adopting a closed-form approach, the performance metrics are further

The current issue and full text archive of this journal is available on Emerald Insight at: **https://www.emerald.com/insight/1708-5284.htm**

World Journal of Engineering
23/2 (2026) 480–492
Emerald Publishing Limited [ISSN 1708-5284]
[DOI 10.1108/WJE-12-2024-0719]



This work was supported by the Tshwane University of Technology, South Africa.

Received 29 December 2024
Revised 20 January 2025
Accepted 14 February 2025

analyzed for the relay position, EH coefficient and signal quality. The outcome of the study reveals the superiority of the TS receivers in comparison to PS receivers. In another related paper (Khennoufa *et al.*, 2023a), the OP and bit error rate (BER) are analyzed for a hybrid PS-TS EH protocol over Nakagami-*m* fading channels. By adopting a closed-form analytical method, it is shown that the proposed solution outperforms the conventional PS and TS signal partitioning methods. In addition to the advantages of reconfigurable intelligent surfaces, the mobile edge computing technology is incorporated in the system model developed in Yang *et al.* (2024). The uniqueness of the study is revealed through the minimized energy consumption and transmission delay.

Owing to the possibility of having multiple relays in CNOMA networks, some studies have also incorporated different relay selection strategies to improve the network performance. In Rahman and Fazlul Kader(2023), the study leverages the amount of harvested energy for selecting the best relay. Moreover, to ensure continuity in transmission while improving the EH rate, the authors explore the possibility where the unselected relays scavenge the energy from the signals transmitted by the selected relay during the second-hop transmission. To further improve the spectrum utilization with minimal latency in CNOMA cognitive radio networks, Huang *et al.* (2023) introduce a signal-to-noise ratio (SNR)-constrained relay selection that determines whether a relay is required to transmit the message of the primary user or not. In addition to the incorporation of relay selection strategy, the study in Panse *et al.* (2023), further incorporates a non-linear EH model and full-duplex (FD) transmission protocol in the study. Findings show that the overall effect of the loop interference and saturation behavior of the circuit leads to an outage floor at the far UE. This finding is further corroborated in Bakshi *et al.* (2024), in addition to the imperfect SIC (i-SIC) that is taken into consideration. In Nagesham and Vappangi (2024), the authors combine the partial RS and optimized PS factor to improve the system BER, OP and throughput.

Another emerging concept introduced in the CNOMA system is the impartial cooperation proposed by Ren *et al.* (2023). This concept allows the near UE and far UE to be used as relays. In addition, the study adopts the Poisson point process to model the distribution of UEs while employing the random and distance-constrained user pairing schemes. Results obtained reveal that the impartial cooperative scheme does not degrade the OP of the system while the nearest-near-nearest-far UE pairing scheme provides the best performance. The effect of i-SIC in addition to the UE pairing on the system achievable rate is investigated in Sreenu and Naidu (2024). Findings show a minor impact of the i-SIC at low transmit power while the achievable rate diminishes at high SNR region due to the severe impact of the i-SIC. Some studies have also prioritized the security aspects of the EH CNOMA networks. In Li *et al.* (2023), the study uses the bit-level exclusive OR and physical-layer network coding encryption techniques to minimize both the intercept and outage probabilities. In addition, the study is investigated under non-linear EH and amplify-and-forward protocols.

Some studies have also incorporated machine learning in the system design to cope with the randomness of the EH environment, such as energy arrival, battery charging and discharging rate and wireless fading channel. In Le *et al.* (2024), the deep neural network (DNN) is used to optimize the network parameters, including the PS factor, rate thresholds, power allocation coefficients and so on. Aside from OP prediction accuracy obtained, the DNN model provides a less complex solution in comparison to the exhaustive search approaches. In Tang *et al.* (2024), the charging and discharging rate of the energy buffer of EH UE is modeled using the finite Markov chain. The study aims to develop a realistic coverage probability for the battery condition of the EH UE. The author of Al Rabee *et al.* (2024) uses the actor-critic method, a variant of deep reinforcement learning, to derive an optimal policy that maximizes the sum data rate. A higher convergence rate is obtained compared with the benchmarks, indicating a less complex solution.

Various realistic designs and optimization approaches have also been introduced to enhance the system performance. In Liu *et al.* (2023), transmit power and time slot allocation are jointly optimized under a non-linear EH condition. The study aims to exploit this strategy to minimize the power consumption at the source. The findings suggest that the source transmit power should be designed around the saturation region of the EH UE. Aside from the non-linear features of EH receivers, the study in Khennoufa *et al.* (2023b) emphasizes that the nonideal phase shifters and mixers used in the RF frontend design are susceptible to in-phase/quadrature-phase imbalance (IQI). Aside from the poor OP at the high SNR due to the higher error floor introduced by imperfect SIC, the presence of the IQI further degrades the OP in this region. In Qian *et al.* (2024), a low-complexity SIC ordering and resource allocation optimization is proposed. While a Lagrangian-based solution is proposed to solve the resource allocation problem, a Tabu search iterative solution is employed to realize a suboptimal SIC ordering. The achieved results in terms of fairness, energy and spectral efficiencies outperform the OMA schemes. In Zhai *et al.* (2024b), a multi-phase adaptive transmission is proposed to improve the success probability of the transmitted message to the destination UE. Further, based on the non-linear EH model, the study adopts a differential evolution algorithm to optimize the power allocation coefficients and the transmission time slot duration.

Meanwhile, the UEs in the aforementioned studies are based on a single-antenna system. Some studies have also incorporated multi-antenna systems in the network design. Yuan *et al.* (2019) solve an energy maximization problem using the optimal parameter values of beamforming vectors and PS factor. In Xu *et al.* (2021), the combined impact of multiple antennas and FD transmission schemes is investigated. In the paper, the optimization of PS ratio and beamforming is performed to maximize the harvested energy. A sub-optimal iterative solution centered on the successive convex approximation method is developed to minimize the computational complexity. To comply with the target rate threshold of a near-field UE, an opportunistic switching between cooperative NOMA and OMA modes is demonstrated in Agrawal *et al.* (2024). In addition to the lower OP achieved, the near UE achieves full diversity, whereas because of the non-linear properties of the EH harvesters, the far UE experiences a loss in diversity. Additional improvement in cognitive CNOMA networks is demonstrated in Salim *et al.* (2024) through the integration of FD transmission and antenna selection. Using the system sum-rate as the main evaluation metric, the system performance is enhanced by adopting particle swarm optimization to tune the power allocation coefficients and PS factor. In Ul Abidin Jaffri and Faheem (2024), the authors introduce the concept of covariance shaping to combat interference from overlapping signals. Based on this, the joint PS ratio, transmit and receive beamforming design is proposed to further reduce the system OP.

To further enhance the effectiveness of cooperative NOMA multi-antenna system, the principle of space-time block coding (STBC) is used to augment the transmit diversity gain. In the STBC scheme, multiple symbols can be transmitted via different antennas over different instants of time (Alamouti, 1998). Hence, this approach can be implemented at the source or the relays when equipped with multiple antennas or via the joint transmission of a single-antenna relays. In Kader and Shin (2017), the OP, ergodic sum-rate and outage sum capacity are analyzed. Aside from the higher performance gain compared with the traditional cooperative NOMA, further findings suggest that an optimal relay position is essential for optimizing the system performance. Akhtar *et al.* (2020) examine the impact of imperfect SIC, CSI and timing synchronization on the system OP. Main findings of the study indicate that the outage performance also reduces with an increase in timing offset. Based on the non-linear properties of EH circuit, the user achievable rate and the network energy efficiency are investigated in our previous work (Alamu *et al.*, 2023c). The study is further extended in Alamu *et al.* (2024) where a multi-user scenario is considered, based on which the system sum-rate is evaluated. In Demirkol *et al.* (2023), the exact OP is derived. Unlike the aforementioned works, the studies demonstrate the impact of receive diversity by equipping the destination UEs with multiple antennas. In Zhai *et al.* (2024a) the authors analyze different relay selection methods. These include random, max-min and max-sum. In the min-max scheme, any relay that satisfies the minimum SNR to detect the transmitted signal is selected, whereas relay selection based on the max-min depends on satisfying the sum-SNR threshold. Findings show that the system throughput under the max-sum scheme outperforms its counterparts.

### 1.1 Motivation and contribution

Given the ever-increasing number of IoT devices, SWIPT-aided cooperative NOMA will be fundamental in enhancing spectral efficiency and seamless connectivity in the next-generation communication systems. Interestingly, several analyses to gauge the performance of cooperative NOMA systems have been conducted, and various improvements have been developed accordingly. Recently, the STBC technique is introduced to further enhance the diversity gain of the destination receivers; however, there are still open areas that can be explored for further improvement. For instance, in Kader and Shin (2017), the study incorporates the STBC scheme at the source and the relay, but EH is not considered at the relay. In Akhtar *et al.* (2020), the STBC transmission is only established via selected single-antenna user-assisted relays with non-consideration of EH. The limitation of Akhtar *et al.* (2020) in terms of EH is addressed in our previous works (Alamu *et al.*, 2023c, 2024), however, the OP and throughput analysis, which are key performance metrics, are not provided. Additionally, these studies rely on specific UEs to carry out the STBC operation, necessitating perfect transmission time synchronization between the selected users. However, this may be difficult to realize in practice compared with the use of a dedicated relay. Moreover, (Akhtar *et al.*, 2020; Alamu *et al.*, 2023c, 2024) do not consider the possibility of implementing the STBC scheme at the source. In Demirkol *et al.* (2023) and Zhai *et al.* (2024a), the studies are based on the nonexistence of a line-of-sight link from the primary transmitter to the relay, a case that is unrealistic in practical scenarios. Therefore, in this study, we aim to address the aforementioned limitations to uncover additional improvements achievable in CNOMA communication systems. To the best of our understanding, no research has yet analyzed the performance of cooperative NOMA with joint consideration of EH at the relay and STBC at the source and the relay. We outline our contributions as follows:

- A CNOMA system is developed comprising a source, a relay and a destination IoT UE. Further, we incorporate the STBC transmission scheme at the source and the relay. The relay is enabled for EH via SWIPT using the gleaned energy from the RF signal to transmit the message of destination UE using a decode-and-forward protocol.
- The direct and cooperative links are modeled based on the independent Rayleigh fading channels. Based on this, we provide a closed-form analysis of the system OP in exact and asymptotic form. Further, the system throughput, energy efficiency and diversity order are examined.
- We compare the numerical results obtained in this study with the baseline schemes. This includes the non-degenerative EH cooperative NOMA, STBC-aided cooperative without EH and incremental conventional cooperative NOMA, among others. Our results show superiority over the baseline approaches.

The structure of the article is as follows: The system modeling and analysis are delineated in Sections 2 and 3, respectively. A discussion of results obtained from the system evaluation is presented in Section 4. We conclude this paper in Section 5, based on the findings of this study.

## 2. System model

Given the illustration in Figure 1, we consider the downlink of a mobile cooperative communication system comprising a Source $S$, Relay $R$ and a destination IoT device $D$. $S$ uses two transmit antennas $S_{tx1}$ and $S_{tx2}$, $R$ uses one receive and two transmit antennas $R_{tx1}$ and $R_{tx2}$ and the $D$ uses one receive antenna. In this study, the location of $D$ is assumed to be at the edge of the network, hence, it may likely experience weak channel conditions as a result of a distance-related pathloss or obstructions in the line-of-sight. Hence, $R$ is installed closer to $S$ and serves as an intermediate device that assists in forwarding the transmitted message from $S$ to $D$. Moreover, $R$ is enabled for EH to replenish its battery using a portion of the signals received from $S$. The channel coefficients from $S$ to $D$, $S$ to $R$ and $R$ to $D$ are represented by $\mathbf{h}_{SD} = \begin{bmatrix} h_1 & h_3 \end{bmatrix}$, $\mathbf{h}_{SR} = \begin{bmatrix} h_2 & h_4 \end{bmatrix}$ and $\mathbf{h}_{RD} = \begin{bmatrix} h_5 & h_6 \end{bmatrix}$, respectively. The complete transmission procedure occurs in two phases, as presented in the following:

### 2.1 Direct phase

Following the Alamouti STBC scheme (Alamouti, 1998), in the first transmission time instance $t_1$, symbols $\begin{bmatrix} x_1 & x_3 \end{bmatrix}^T$ and $\begin{bmatrix} x_2 & x_4 \end{bmatrix}^T$ corresponding to $S_{tx1}$ and $S_{tx2}$ are transmitted to $D$ and $R$, respectively. However, since superimposed signal is

**Figure 1** A CNOMA system with STBC transmission scheme

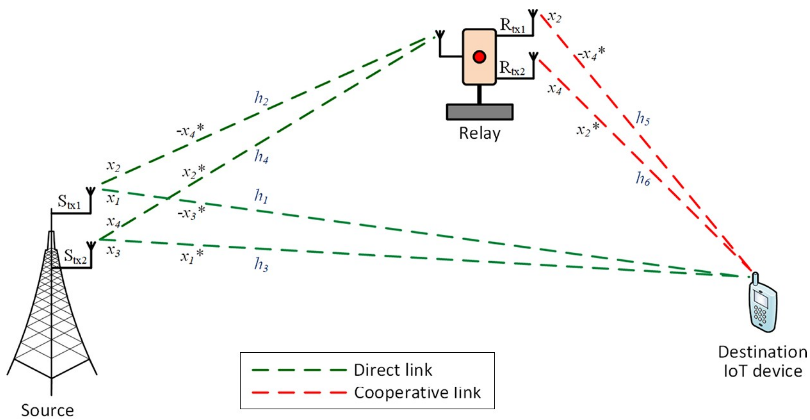


**Source(s):** Authors' own work

transmitted in NOMA scheme, $D$ and $R$ also receive a copy of $\left[x_2 \quad x_4\right]^T$ and $\left[x_1 \quad x_3\right]^T$, respectively. Hence, in the direct transmission phase, $D$ and $R$ receive the transmit signals given in equations (1) and (2), respectively.

$$y_D^{t_1} = \sqrt{P_0}\left(h_1\left[\sqrt{\alpha_D}x_1 + \sqrt{\alpha_R}x_2\right] + h_3\left[\sqrt{\alpha_D}x_3 + \sqrt{\alpha_R}x_4\right]\right) + n_D, \quad (1)$$

$$y_D^{t_1} = \sqrt{(1-\rho)P_0}\left(h_2\left[\sqrt{\alpha_R}x_2 + \sqrt{\alpha_D}x_1\right] + h_4\left[\sqrt{\alpha_R}x_4 + \sqrt{\alpha_R}x_3\right]\right) + n_R. \quad (2)$$

We denote the transmission power at the source as $P_0$. The power allocation factors assigned to $D$ and $R$ are denoted as $\alpha_D$ and $\alpha_R$, respectively, satisfying $\alpha_D > \alpha_R > 0$ and $\alpha_D + \alpha_R = 1$. The relay uses a fraction, i.e. $(1-\rho)$ of the received signal for decoding its message symbols. The PS factor is denoted by $\rho$. The parameters $n_D \sim \mathcal{CN}\left(0, \sigma_D^2\right)$ and $n_R \sim \mathcal{CN}\left(0, \sigma_R^2\right)$ represent the additive white Gaussian noise introduced by the receivers of $D$ and $R$, respectively.

In the second transmission time instance $t_2$, the conjugate of symbols $\left[x_1 \quad x_3\right]^T$ i.e. $\left[-x_3^* \quad x_1^*\right]^T$ and the conjugate of symbols $\left[x_2 \quad x_4\right]^T$, i.e. $\left[-x_4^* \quad x_2^*\right]^T$ corresponding to $S_{tx1}$ and $S_{tx2}$ are transmitted to $D$ and $R$, respectively. Here, the received signals at $D$ and $R$ are expressed in equations (3) and (4), respectively.

$$y_D^{t_2} = \sqrt{P_0}\left(-h_1\left[\sqrt{\alpha_D}x_3^* + \sqrt{\alpha_R}x_4^*\right] + h_3\left[\sqrt{\alpha_D}x_1^* + \sqrt{\alpha_R}x_2^*\right]\right) + n_D, \quad (3)$$

$$y_R^{t_2} = \sqrt{(1-\rho)P_0}\left(-h_2\left[\sqrt{\alpha_R}x_4^* + \sqrt{\alpha_D}x_3^*\right] + h_4\left[\sqrt{\alpha_R}x_2^* + \sqrt{\alpha_D}x_1^*\right]\right) + n_R. \quad (4)$$

The encoding and transmission sequence adopted in equations (1) to (4) are summarized in Table 1. Here, $z_{s1}$ and $z_{s2}$ and their corresponding conjugates $-z_{s2}^*$ and $z_{s1}^*$ denote the composite signals received at $D$ and $R$, respectively, from $S_{tx1}$ and $S_{tx2}$ during the two transmission time instances $t_1$ and $t_2$.

Therefore, the signal-to-interference plus noise ratio (SINR) received at $D$ to detect its message symbols can be written as:

$$\gamma_{SD} = \frac{\alpha_D \frac{P_0}{2}\left\|\mathbf{h}_{SD}\right\|^2}{\alpha_R \frac{P_0}{2}\left\|\mathbf{h}_{SD}{}^2\right\| + \sigma_D^2}. \quad (5)$$

Equation (5) can further be simplified as:

$$\gamma_{SD} = \frac{\alpha_D \beta \left\|\mathbf{h}_{SD}\right\|^2}{\alpha_R \beta \left\|\mathbf{h}_{SD}\right\|^2 + 1} \quad (6)$$

where $\beta = \frac{P_0}{2\,\sigma_{SD}^2}$ denotes the input SNR.

At the relay, the SINR to detect the interfering symbols of $D$ is given as:

$$\gamma_{SD \to D} = \frac{(1-\rho)\alpha_D \beta \left\|\mathbf{h}_{SR}\right\|^2}{(1-\rho)\alpha_R \beta \left\|\mathbf{h}_{SR}\right\|^2 + 1} \quad (7)$$

Further, $R$ uses SIC to nullify the interfering symbols of $D$. Hence, the received SNR at $R$ from $S$ after performing the SIC operation can be written as:

$$\gamma_{SR} = (1-\rho)\alpha_R \beta \left\|\mathbf{h}_{SR}\right\|^2. \quad (8)$$

Furthermore, $R$ performs EH from the signal received from $S$ and the harvested power can be computed as:

$$P_R = \zeta \rho \beta \left\|\mathbf{h}_{SR}\right\|^2, \quad (9)$$

where $\zeta$ is the energy conversion efficiency.

### 2.2 Cooperative phase

In the cooperative phase, $R$ applies decode-and-forward protocol and STBC scheme to re-transmit $\left[x_2 \quad x_4\right]^T$ to $D$. Therefore, the received signal at $D$ during the two time instances, denoted by $t_3$ and $t_4$, can be written as given in equations (10) and (11), respectively:

$$y_{RD}^{t_3} = \sqrt{P_R}\left(h_5 x_2 + h_6 x_4\right) + n_D \quad (10)$$

$$y_{RD}^{t_4} = \sqrt{P_R}\left(-h_5 x_4^* + h_6 x_2^*\right) + n_D. \quad (11)$$

**Table 1** STBC Transmission scheme for EH CNOMA

| Time | $S_{tx1}$ | $S_{tx2}$ |
|---|---|---|
| $t_1$ | $z_{s1} = \sqrt{\alpha_D}x_1 + \sqrt{\alpha_R}x_2$ | $z_{s2} = \sqrt{\alpha_D}x_3 + \sqrt{\alpha_R}x_4$ |
| $t_2$ | $-z_{s2}^* =- \sqrt{\alpha_D}x_3^* - \sqrt{\alpha_R}x_4^*$ | $z_{s1}^* = \sqrt{\alpha_D}x_1^* + \sqrt{\alpha_R}x_2^*$ |

**Source:** Authors' own work

Accordingly, $D$ receives the SNR in equation (12) to decode its message:

$$\gamma_{RD} = \zeta\rho\frac{\beta}{2}\|\mathbf{h}_{SR}\|^2\|\mathbf{h}_{SD}\|^2 \tag{12}$$

The SNR received in the direct and cooperative phases are aggregated at $D$ the using maximum ratio combining (MRC) method. Therefore, we have the total SNR at $D$ as:

$$\gamma_D^{MRC} = \frac{\alpha_D\beta\|\mathbf{h}_{SD}\|^2}{\alpha_R\beta\|\mathbf{h}_{SD}\|^2 + 1} + \zeta\rho\frac{\beta}{2}\|\mathbf{h}_{SR}\|^2\|\mathbf{h}_{SD}\|^2. \tag{13}$$

## 3. Performance analysis

Here, we present the analytical expressions to gauge the effectiveness of the proposed system model. These include the OP and throughput analysis.

### 3.1 Outage probability analysis of destination user equipment

Here, we denote the target data rates for $D$ and $R$ with $R_D$ and $R_R$, respectively. Therefore, the minimum SNRs needed by $R$ corresponding to equations (7) and (8) can be further expressed as $\tau_D = 2^{2\mathcal{R}_\mathcal{D}} - 1 = \gamma_{SR\to D}$ and $\tau_R = 2^{2\mathcal{R}_\mathcal{R}} - 1 = \gamma_{SR}$, respectively. Hence, after some algebraic manipulations, the fair power allocation factors and PS factor can be derived as given in equations (14), (15) and (16), respectively:

$$\alpha_R^* = \frac{\tau_R}{\psi}, \tag{14}$$

$$\alpha_D^* = 1 - \alpha_R^*, \tag{15}$$

$$\rho^* = \max\{0, \rho\}, \tag{16}$$

where $\psi = 2^{2(\mathcal{R}_\mathcal{R} + \mathcal{R}_\mathcal{D})} - 1$ and $\rho = 1 - \frac{\psi}{\beta\|\mathbf{h}_{SR}\|^2}$.

In this study, it is assumed that $R$ is only active when $\rho^* > 0$, and inactive when $\rho^* = 0$. Therefore, in the latter case, the system is enabled to degenerate into traditional non-cooperative NOMA transmission to optimize the time resources. Thus, rather than permitting the time designated for the cooperative phase to remain unutilized, the entire time slot can be used for direct transmission. Hence, equations (7) and (8) become (17) and (18), respectively:

$$\gamma'_{SR\to D} = \frac{\alpha_D\beta\|\mathbf{h}_{SR}\|^2}{\alpha_R\beta\|\mathbf{h}_{SR}\|^2 + 1}, \tag{17}$$

$$\gamma'_{SR\to D} = \alpha_R\beta\|\mathbf{h}_{SR}\|^2. \tag{18}$$

Following the same approach used in the derivation of (14) and (15), i.e. setting $\tau'_D = 2^{\mathcal{R}_\mathcal{D}} - 1 = \gamma'_{SR\to D}$ and $\tau'_R = 2^{\mathcal{R}_\mathcal{R}} - 1 = \gamma'_{SR}$, the power allocation factors can be given as $\alpha'_R = \frac{\tau'_R}{\psi'}$ and $\alpha'_D = 1 - \alpha'_R$, respectively, where $\psi' = 2^{\mathcal{R}_\mathcal{R} + \mathcal{R}_\mathcal{D}} - 1$. Therefore, the OP expression at $D$ can be written as:

$$P_{\text{out}}^D = \underbrace{\Pr\left\{\gamma_{SD}|_{\rho^*=0} < \tau'_D\right\}\Pr\{\rho^* = 0\}}_{P_{out}^{D1}} + \underbrace{\Pr\left\{\gamma_D^{MRC}|_{\rho^*>0} < \tau_D\right\}\Pr\{\rho^* > 0\}}_{P_{out}^{D2}}, \tag{19}$$

where $P_{out}^{D1}$ and $P_{out}^{D2}$ represent the OP of $D$ in the direct phase and indirect phase respectively.

Using the notations $X = \|\mathbf{h}_{SD}\|^2$, $Y = \|\mathbf{h}_{SR}\|^2$ and $Z = \|\mathbf{h}_{RD}\|^2$, we denote the corresponding mean channel gains as $L\mu_1$, $L\mu_2$ and $L\mu_3$, respectively. Note that $X$, $Y$ and $Z$ follow the chi-square distribution with the degree of freedom $2L$ (Björnson and Demir, 2024), with their probability density functions given in equations (20), (21) and (22), as:

$$f_{\|\mathbf{h}_{SD}\|^2}(x) = \frac{x^{L-1}}{\mu_1^L(L-1)!}e^{-\frac{x}{\mu_1}}, \tag{20}$$

$$f_{\|\mathbf{h}_{SR}\|^2}(y) = \frac{y^{L-1}}{\mu_2^L(L-1)!}e^{-\frac{y}{\mu_2}}, \tag{21}$$

$$f_{\|\mathbf{h}_{RD}\|^2}(z) = \frac{z^{L-1}}{\mu_3^L(L-1)!}e^{-\frac{z}{\mu_3}}, \tag{22}$$

respectively, where $L$ is the number of transmission antennas. Therefore, we can write the OP at $D$ as:

$$\begin{aligned} P_{out}^D &= \left(1 - e^{-\frac{\psi'}{\mu_1\beta}}\sum_{l=0}^{L-1}\frac{\left(\frac{\psi'}{\mu_1\beta}\right)^l}{l!}\right)\left(1 - e^{-\frac{\psi}{\mu_2\beta}}\sum_{l=0}^{L-1}\frac{\left(\frac{\psi}{\mu_2\beta}\right)^l}{l!}\right) \\ &+ \frac{1}{\mu_1\mu_2}\left(\sum_{l=0}^{L-1}\frac{1}{\mu_1^l\mu_2^l(l!)^2}\right)^2\left(\frac{e^{-\frac{\psi}{\mu_2\beta}}}{\beta^{l+1}}\sum_{n=0}^{l}\binom{l}{n}\psi^{l-n}(\mu_2\beta)^{n-k+1}\,\Gamma(n-k+1)\right) \\ &\times\left(\frac{2}{\mu_3\zeta}\left(\frac{\psi}{\beta}\mu_1^{l+1}\gamma\left(l+1,\frac{\psi}{\beta\mu_1}\right) - \alpha_D^*\beta\mu_1^{l+2}\gamma\left(l+2,\frac{\psi}{\beta\mu_1}\right)\right)\right). \end{aligned} \tag{23}$$

*Proof:* First, let's consider $P_{out}^{D1}$ in equation (19), which is given as:

$$P_{\text{out}}^{D1} = \underbrace{\Pr\left\{\|\boldsymbol{h}_{\text{SD}}\|^2 < \frac{\psi'}{\beta}\right\}}_{P_{\text{out}}^{D1,1}}\underbrace{\Pr\left\{\|\boldsymbol{h}_{SR}\|^2 < \frac{\psi}{\beta}\right\}}_{P_{\text{out}}^{D1,2}} \tag{24}$$

From equation (24), $P_{out}^{D1,1}$ can be computed as:

$$P_{out}^{D1,1} = \int_0^{\frac{\psi'}{\beta}}\frac{x^{L-1}}{\mu_1^L(L-1)!}e^{-\frac{x}{\mu_1}}\partial x, \tag{25}$$

$$=\left[-\frac{\mu_1 x^{L-1}e^{-\frac{x}{\mu_1}}}{\mu_1^L(L-1)!}\right]_0^{\frac{\psi'}{\beta}}+\int_0^{\frac{\psi'}{\beta}}\frac{\mu_1(L-2)x^{L-1}e^{-\frac{x}{\mu_1}}}{\mu_1^L(L-1)!}\partial x, \quad (26)$$

$$=\left[-\frac{x^{L-1}e^{-\frac{x}{\mu_1}}}{\mu_1^{L-1}(L-1)!}\right]_0^{\frac{\psi'}{\beta}}+\int_0^{\frac{\psi'}{\beta}}\frac{x^{L-1}e^{-\frac{x}{\mu_1}}}{\mu_1^{L-1}(L-2)!}\partial x, \quad (27)$$

$$=-\frac{\left(\frac{\psi'}{\beta}\right)^{L-1}e^{-\frac{\psi'}{\mu_1\beta}}}{\mu_1^{L-1}(L-1)!}+\int_0^{\frac{\psi'}{\beta}}\frac{x^{L-1}e^{-\frac{x}{\mu_1}}}{\mu_1^{L-1}(L-2)!}\partial x. \quad (28)$$

Note that the integration operation is performed again on the second right-hand side (RHS) term of equation (28), i.e. $\int_0^{\frac{\psi'}{\beta}}\frac{x^{L-1}e^{\frac{x}{\mu_1}}}{\mu_1^{L-1}(L-2)!}\partial x$. Hence, the final expression after performing several repetitions of the integration operation can be given as:

$$P_{out}^{D1,1}=\left(1-e^{-\frac{\psi'}{\mu_1\beta}}\sum_{l=0}^{L-1}\frac{\left(\frac{\psi'}{\mu_1\beta}\right)^l}{l!}\right) \quad (29)$$

Similarly, $P_{out}^{D1,2}$ in equation (24) can be expressed:

$$P_{out}^{D1,2}=\left(1-e^{-\frac{\psi}{\mu_2\beta}}\sum_{l=0}^{L-1}\frac{\left(\frac{\psi}{\mu_2\beta}\right)^l}{l!}\right). \quad (30)$$

Therefore,

$$P_{out}^{D1}=\left(1-e^{-\frac{\psi'}{\mu_1\beta}}\sum_{l=0}^{L-1}\frac{\left(\frac{\psi'}{\mu_1\beta}\right)^l}{l!}\right)\left(1-e^{-\frac{\psi}{\mu_2\beta}}\sum_{l=0}^{L-1}\frac{\left(\frac{\psi}{\mu_2\beta}\right)^l}{l!}\right). \quad (31)$$

The proof is completed.

*Corollary:* From equations (24), in high SNR, i.e. $\frac{1}{\beta}=\frac{1}{\infty}\approx 0$, the terms $e^{-\frac{x}{\mu_1}}=1$ in equations (25). Therefore, the asymptotic expression of $P_{out}^{D1}$ i.e. $P_{out}^{D1}|_{\beta\to\infty}$ can be derived as:

$$P_{out}^{D1}|_{\beta\to\infty}=\frac{1}{(L!)^2}\left(\frac{\psi'\psi}{\mu_1\mu_2\beta^2}\right)^L \quad (32)$$

Proof: Consider $P_{\text{out}}^{\text{D1,1}}|_{\beta\to\infty}$ which can be given as:

$$P_{out}^{D1,1}|_{\beta\to\infty}=\int_0^{\frac{\psi'}{\beta}}\frac{x^{L-1}}{\mu_1^L(L-1)!}\partial x \quad (33)$$

$$=\left[\frac{x^L}{\mu_1 L(L-1)!}\right]_0^{\frac{\psi'}{\beta}}, \quad (34)$$

$$=\frac{1}{L!}\left(\frac{\psi'}{\mu_1\beta}\right)^L. \quad (35)$$

Similarly, $P_{out}^{D1,2}|_{\beta\to\infty}$ can be given as:

$$P_{out}^{D1,2}|_{\beta\to\infty}=\frac{1}{L!}\left(\frac{\psi}{\mu_2\beta}\right)^L. \quad (36)$$

Therefore, the final expression for $P_{out}^{D1}|_{\beta\to\infty}$ can be given as:

$$P_{out}^{D1}|_{\beta\to\infty}=\frac{1}{(L!)^2}\left(\frac{\psi'\psi}{\mu_1\mu_2\beta^2}\right)^L. \quad (37)$$

The proof is completed.

Considering $P_{out}^{D2}$ in equations (19) which can be expressed as:

$$P_{out}^{D2}=\Pr\left\{\frac{\alpha_D^*\beta\|\boldsymbol{h}_{SD}\|^2}{\alpha_R^*\beta\|\boldsymbol{h}_{SD}\|^2+1}+\zeta\rho^*\frac{\beta}{2}\|\boldsymbol{h}_{SR}\|^2\|\boldsymbol{h}_{RD}\|^2<\frac{\psi}{\beta}\right\}\Pr\left\{\|\boldsymbol{h}_{SR}\|^2>\frac{\psi}{\beta}\right\}, \quad (38)$$

$$=\Pr\left\{\frac{\alpha_D^*\beta\|\boldsymbol{h}_{SD}\|^2}{\alpha_R^*\beta\|\boldsymbol{h}_{SD}\|^2+1}+\frac{\zeta}{2}\left(\beta\|\boldsymbol{h}_{SR}\|^2-\psi\right)\|\boldsymbol{h}_{RD}\|^2<\frac{\psi}{\beta}\right\}\Pr\left\{\|\boldsymbol{h}_{SR}\|^2>\frac{\psi}{\beta}\right\}, \quad (39)$$

$$=\Pr\left\{\|\boldsymbol{h}_{RD}\|^2<\frac{\frac{\psi}{\beta}-\frac{\alpha_D^*\beta\|\boldsymbol{h}_{SD}\|^2}{\alpha_R^*\beta\|\boldsymbol{h}_{SD}\|^2+1}}{\frac{\zeta}{2}\left(\beta\|\boldsymbol{h}_{SR}\|^2-\psi\right)}\right\}\Pr\left\{\|\boldsymbol{h}_{SD}\|^2<\frac{\psi}{\beta}\right\}\Pr\left\{\|\boldsymbol{h}_{SR}\|^2>\frac{\psi}{\beta}\right\}, \quad (40)$$

$$=\frac{1}{\mu_1\mu_2}\int_0^{\frac{\psi}{\beta}}\int_{\frac{\psi}{\beta}}^{\infty}\left(1-e^{-\frac{\frac{\psi}{\beta}-\frac{\alpha_D^*\beta x}{\alpha_R^*\beta x+1}}{\mu_2(\beta y-\psi)}}\right)e^{-\frac{x}{\mu_1}}\sum_{l=0}^{L-1}\frac{\left(\frac{x}{\mu_1}\right)^l}{l!}e^{-\frac{y}{\mu_2}}\sum_{l=0}^{L-1}\frac{\left(\frac{y}{\mu_2}\right)^l}{l!}\,\mathrm{d}y\mathrm{d}x, \quad (41)$$

$$=\frac{1}{\mu_1\mu_2}\left(\sum_{l=0}^{L-1}\frac{1}{\mu_1^l\mu_2^l(l!)^2}\right)^2\int_0^{\frac{\psi}{\beta}}x^l e^{-\frac{x}{\mu_1}}\int_{\frac{\psi}{\beta}}^{\infty}y^l e^{-\frac{y}{\mu_2}}\left(1-e^{-\frac{\frac{\psi}{\beta}-\frac{\alpha_p^*\beta x}{\alpha_R^*\beta x+1}}{\frac{\zeta}{2}(\beta y-\psi)}}\right)\mathrm{d}y\mathrm{d}x, \quad (42)$$

$$=\frac{1}{\mu_1\mu_2}\left(\sum_{l=0}^{L-1}\frac{1}{\mu_1^l\mu_2^l(l!)^2}\right)^2\int_0^{\frac{\psi}{\beta}}x^l e^{-\frac{x}{\mu_1}}\underbrace{\int_0^{\infty}\left(\frac{u+\psi}{\beta}\right)^l\frac{e^{-\frac{\psi}{\mu_2\beta}}}{\beta}\left(1-e^{-\frac{\frac{\psi}{\beta}-\frac{\alpha_R^*\beta x}{\alpha_R^*\beta x+1}}{\frac{\mu_3\zeta}{2}u}}\right)e^{-\frac{u}{\mu_2\beta}}\mathrm{d}u\mathrm{d}x}_{I_{in}}. \quad (43)$$

Note that the expression $\|\mathbf{h}_{RD}\|^2<\frac{\frac{\psi}{\beta}-\frac{\alpha_D^*\beta\|\mathbf{h}_{SD}\|^2}{\alpha_R^*\beta\|\mathbf{h}_{SD}\|^2+1}}{\frac{\zeta}{2}\left(\beta\|\mathbf{h}_{SR}\|^2-\psi\right)}$, in the equation (40) holds based on the argument that, $\mathbb{E}\left\{\frac{\alpha_D^*\beta\|\mathbf{h}_{SD}\|^2}{\alpha_R^*\beta\|\mathbf{h}_{SD}\|^2+1}\right\}<\frac{\psi}{\beta}$ thus, the reason for the additional term $\|\mathbf{h}_{SD}\|^2<\frac{\psi}{\beta}$. Factorizing

equation (41) we obtain equation (42) and using the reverse chain rule, $u = \beta y - \psi$, we derive equation (43).
From equations (43), we have:

$$I_{\text{in}} = \int_0^\infty \left(\frac{u+\psi}{\beta}\right)^l \frac{e^{-\frac{\psi}{\mu_2\beta}}}{\beta}\left(1 - e^{-\frac{\frac{\psi}{\beta}-\frac{\alpha_D^*\beta x}{\alpha_R^*\beta x+1}}{\frac{\mu_3\zeta}{2}u}}\right) e^{-\frac{u}{\mu_2\beta}}\mathrm{d}u \tag{44}$$

$$\approx \frac{e^{-\frac{\psi}{\mu_2\beta}}}{\beta}\int_0^\infty \left(\frac{u+\psi}{\beta}\right)^l \left(\frac{\frac{\psi}{\beta}-\frac{\alpha_D^*\beta x}{\alpha_R^*\beta x+1}}{\frac{\mu_3\zeta}{2}u} - \frac{1}{2}\left(\frac{\frac{\psi}{\beta}-\frac{\alpha_D^*\beta x}{\alpha_R^*\beta x+1}}{\frac{\mu_3\zeta}{2}u}\right)^2\right) e^{-\frac{u}{\mu_2\beta}}\mathrm{d}u, \tag{45}$$

$$\approx \frac{e^{-\frac{\psi}{\mu_2\beta}}}{\beta^{l+1}}\sum_{n=0}^{l}\binom{l}{n}\psi^{l-n}\int_0^\infty u^n \left(\frac{\frac{\psi}{\beta}-\frac{\alpha_D^*\beta x}{\alpha_R^*\beta x+1}}{\frac{\mu_3\zeta}{2}u} - \frac{1}{2}\left(\frac{\frac{\psi}{\beta}-\frac{\alpha_D^*\beta x}{\alpha_R^*\beta x+1}}{\frac{\mu_3\zeta}{2}u}\right)^2\right) e^{-\frac{u}{\mu_2\beta}}\mathrm{d}u, \tag{46}$$

$$\approx \frac{e^{-\frac{\psi}{\mu_2\beta}}}{\beta^{l+1}}\sum_{n=0}^{l}\binom{l}{n}\psi^{l-n}(\mu_2\beta)^{n-k+1}\,\Gamma(n-k+1)\left(\frac{\frac{\psi}{\beta}-\frac{\alpha_D^*\beta x}{\alpha_R^*\beta x+1}}{\frac{\mu_3\zeta}{2}u}\right). \tag{47}$$

The expanded series of the $1 - e^{-\frac{\frac{\psi}{\beta}-\frac{\alpha_D^*\beta x}{\alpha_R^*\beta x+1}}{\frac{\mu_3\zeta}{2}u}}$ in the truncated form is given in equation (45). Invoking the Binomial theorem to handle the term $\left(\frac{u+\psi}{\beta}\right)^l$, we obtain equation (46). In equation (47), note that the series terms can be written in the form of $\int_0^\infty \frac{1}{u^k} e^{-\frac{u}{\mu_2\beta}}\mathrm{d}u$ for k = 1, 2, …, and simplifying using $\int_0^\infty t^{z-1}e^{-1}\mathrm{d}t = \Gamma(z)$ (Zwillinger and Jeffrey, 2000).
Let $I_{out}$ denote the outer integral in equation (43) thus from equation (47) we have,

$$I_{out} = \int_0^{\frac{\psi}{\beta}} x^l e^{-\frac{x}{\mu_1}}\left(\frac{\frac{\psi}{\beta}-\frac{\alpha_D^*\beta x}{\alpha_R^*\beta x+1}}{\frac{\mu_3\zeta}{2}u}\right)\mathrm{d}x \tag{48}$$

$$= \frac{2}{\mu_3\zeta}\int_0^{\frac{\psi}{\beta}} x^l e^{-\frac{x}{\mu_1}}\left(\frac{\psi}{\beta} - \frac{\alpha_D^*\beta x}{\alpha_R^*\beta x+1}\right)\mathrm{d}x, \tag{49}$$

$$\approx \frac{2}{\mu_3\zeta}\left(\frac{\psi}{\beta}\mu_1^{l+1}\gamma\left(l+1,\frac{\psi}{\beta\mu_1}\right) - \alpha_D^*\beta\mu_1^{l+2}\gamma\left(l+2,\frac{\psi}{\beta\mu_1}\right)\right), \tag{50}$$

where the lower incomplete Gamma function is denoted by $\gamma$. Also, note that to realize the final expression in equation (50), the term $\frac{\alpha_D^*\beta x}{\alpha_R^*\beta x+1}$ is approximated via truncated Taylor series expansion as $\alpha_D^*\beta x\left(1 - \alpha_R^* + (\alpha_R^*\beta x)^2\right)$.
Hence, the final expression can be written as:

$$P_{\text{out}}^{D2} = \frac{1}{\mu_1\mu_2}\left(\sum_{L-1}^{l=0}\frac{1}{\mu_1^l\mu_2^l(l!)^2}\right)^2 \left(\frac{e^{-\frac{\psi}{\mu_2\beta}}}{\beta^{l+1}}\sum_{n=o}^{l}\binom{l}{n}\psi^{l-n}(\mu_2\beta)^{n-k+1}\,\Gamma(n-k+1)\right)$$
$$\times\left(\frac{2}{\mu_3\zeta}\left(\frac{\psi}{\beta}\mu_1^{l+1}\gamma\left(l+1,\frac{\psi}{\beta\mu_1}\right) - \alpha_D^*\beta\mu_1^{l+2}\gamma\left(l+2,\frac{\psi}{\beta\mu_1}\right)\right)\right) \tag{51}$$

In the high SNR region, the expression in equation (51) is dominated by the $\frac{1}{\beta^{l+1}}$ from the second term in the RHS. Hence, the asymptotic expression can be approximated as:

$$P_{out}^{D2}|_{\beta\to\infty} \approx \frac{1}{\mu_1\mu_2}\left(\sum_{l=0}^{L-1}\frac{1}{\mu_1^l\mu_2^l(l!)^2}\right)^2\frac{1}{\beta^{l+1}}. \tag{52}$$

### 3.2 Outage probability analysis of the relay

The relay $R$ is in outage if it cannot harvest energy (i.e. $\rho^* = 0$) or is unable to decode its message and that of the destination UE $D$. An intuitive approach to analyze the latter cases is to modify the expression in equation (16) with respect to $\psi'$ and set $\rho^* = 0$. Hence, the OP expression in this case, following the approach in the derivation of equation (29), can be written as:

$$P_{out}^R = Pr\left\{\gamma'_{SR\to D}|_{\rho^*=0} < \tau'_D \;\; or \;\; \gamma'_{SR}|_{\rho^*=0} < \tau'_R\right\}Pr\{\rho^*=0\}, \tag{53}$$

$$= \Pr\left\{\|\mathbf{h}_{SR}\|^2 < \frac{\psi'}{\beta}\right\}\Pr\left\{\|\mathbf{h}_{SR}\|^2 < \frac{\psi}{\beta}\right\} \tag{54}$$

$$= \left(1 - e^{-\frac{\psi'}{\mu_2\beta}}\sum_{l=0}^{L-1}\frac{\left(\frac{\psi'}{\mu_2\beta}\right)^l}{l!}\right) \tag{55}$$

We obtain the expression in equation (55) because $\psi' = \psi$, which indicates the minimum target rate for $R$ to be in an outage.
In the high SNR region, following the approach in the derivation of equation (35), $P_{out}^R|_{\beta\to\infty}$

$$P_{out}^R|_{\beta\to\infty} = \frac{1}{L!}\left(\frac{\psi'}{\mu_2\beta}\right)^L \tag{56}$$

### 3.3 Throughput analysis

Given the achievable data rate threshold $\mathcal{B}_{\mathcal{D}}$, and $\mathcal{B}_{\mathcal{B}}$, the system throughput can be computed as given equation (57).

$$T_s = \left(1 - P_{\text{out}}^D\right)\mathcal{R}_{\mathcal{D}} + \left(1 - P_{\text{out}}^R\right)\mathcal{R}_{\mathcal{R}}. \tag{57}$$

### 3.4 Energy efficiency

Here, we analyze the energy efficiency of the developed system. Energy efficiency can be defined as the ratio of the sum-rate in the system to the total power consumed in the system. This can be given as

$$\text{Energy efficiency} \quad = \frac{\widetilde{\mathcal{R}}_{\mathcal{D}} + \widetilde{\mathcal{R}}_{\mathcal{R}}}{\xi P_0 + P_0^c + P_R^c + P_D^c - P_R}, \quad (58)$$

where $\widetilde{\mathcal{R}}_{\mathcal{D}}$ and $\widetilde{\mathcal{R}}_{\mathcal{R}}$, given in (59) and (60), are the achievable rates of the destination devices and the relay, respectively. $P_D^c$ and $P_R^c$ denote the power consumed in the circuit of the destination UE and the relay, respectively.

$$\widetilde{\mathcal{R}}_{\mathcal{D}} = \frac{1}{2}\log_2\left(1 + \frac{\alpha_D\beta\|\mathbf{h}_{SD}\|^2}{\alpha_R\beta\|\mathbf{h}_{SD}\|^2 + 1} + \zeta\rho\frac{\beta}{2}\|\mathbf{h}_{SR}\|^2\|\mathbf{h}_{SD}\|^2\right), \quad (59)$$

$$\widetilde{\mathcal{R}}_{\mathcal{R}} = \frac{1}{2}\log_2\left(1 + (1-\rho)\alpha_R\beta\|\mathbf{h}_{SR}\|^2\right) \quad (60)$$

### 3.5 Diversity order analysis

To provide the closed-form diversity order analysis at $D$ we use its asymptotic OP expressions. Hence, we compute the diversity order as:

$$\widehat{D}_{\mathcal{D}} = -\lim_{\beta\to\infty}\frac{\log P_{out}^D}{\log\beta} \quad (61)$$

Focusing on the term with $\beta$ in equations (37) and (52), we have $\left(\frac{\psi^{'}\psi}{\mu_1\mu_2\beta^2}\right)^L$ and $\frac{1}{\beta^{l+1}}$, respectively. The former term scales as $\beta^{-2L}$ while we have $\beta^{(l+1)}$ in the latter. Therefore, the scaling product in terms of $\beta$ can be given as:

$$\beta^{-2L}.\beta^{-(l+1)} = \beta^{-(2L+l+1)}. \quad (62)$$

Note that since $l \in [0, L-1]$, the expression in equation (62) term is bounded $l = L-1$. Therefore, we have the dominant scaling factor as $L$, if we consider the largest $l+1$ value. Thus, equation (62) can be reduced to $\beta^{-3L}$. In this paper, the transmission links $L_{S\text{–}D} = L_{R\text{–}D} = 2$. Finally, the expression for the diversity order can be given as:

$$\widehat{D}_{\mathcal{D}} = 3L = 6. \quad (63)$$

Similarly, the diversity order at the relay can be computed as:

$$\widehat{D}_R = -\lim_{\beta\to\infty}\frac{\log P_{out}^R}{\log\beta} \quad (64)$$

Using the same approach in analysing $\widehat{D}_{\mathcal{D}}$, we can compute $\widehat{D}_R$ from equation (56) by focusing on the term with $\beta$ i.e. $\left(\frac{\psi^{'}}{\mu_2\beta}\right)^L$. Thus, we have $\beta^{-L}$ and its corresponding diversity order is $\widehat{D}_R = L = 2$.

### 3.6 Complexity analysis

Here, we examine the complexity of the proposed solution based on different operations performed at the source and receivers of the relay and destination UE. These operations include STBC transmission, SIC, EH and MRC. For the STBC encoding, four-symbol blocks are required at the source as indicated in Table 1, while two-symbol blocks are needed at the relay as given in equation (10) and (11) (Wang *et al.*, 2006). Hence, we have $O(3T)$, when half of the time is allocated for direct transmission. For the decoding part, the operation requires $O(n_r n_t T)$, where the number of transmit and receive antennas is denoted by $n_r$ and $n_t$, respectively. Hence, for decoding at the relay and the destination UE, each incurs a complexity of $O(2T)$. Therefore, the total STBC encoding and decoding phases are $O(5T)$. In the SIC phase, the complexity is mainly due to the contributions from the relay (Xu *et al.*, 2023), as the destination or far-field UE in NOMA treats the interfering signal as noise. Hence we have $O(n_r \log n_r)$ for inter-user interference cancelation and $O(3K \log M)$ per UE, where $M$ and $K$ are the modulation order and number of UEs, respectively. Thus, the SIC complexity can be given as $O(4 \log M)$. For the MRC operation, the complexity is $O(L)$, as $L$ multiplication and $L-1$ addition operations are required. In this case, we have $O(4)$. The complexity of EH operation can be given as $O(N\Delta C)$, where $N$, $\Delta$ and $C$, are the number of relays, number of conditional loops for the degenerative process and cost of harvested energy, respectively. The cost of harvested energy is equivalent to $P_R.T$, where $P_R$ is given in (9). Thus, we have $O(5T) + O(2 \log M) + O(4) + O(\Delta C)$ as the total complexity of the system.

## 4. Numerical results and discussion

Here, the analytical results are presented, which are validated via simulations in MATLAB. The channel gains are modeled as $\mu_1 = d_1^{-\Omega}$, $\mu_2 = d_2^{-\Omega}$ and $\mu_3 = d_3^{-\Omega}$, where $d_1 = 10$ m, is the distance between $S$ and $D$, $d_2 = 4$ m, is the distance from $S$ to $R$, and $d_3 = d_1 - d_2$ is the distance between $R$ and $D$. The pathloss exponent is denoted by $\Omega$. The power allocation factors $\alpha_D = 0.8$ and $\alpha_R = 0.2$. The energy conversion efficiency is $\zeta = 0.7$, and the PS factor $\rho = 0.4$. The noise power $\sigma_D^2 = \sigma_R^2 = -90$ dBm. The circuit power consumption values $P_0^c$, $P_R^c$ and $P_D^c$ is 5 dBm, 10 dBm and 40 dBm, respectively. The power amplification constant is $\xi = 0.4$. Further, we benchmark our findings with other transmission strategies as described in the following:

- *EH CC-NOMA-STBC:* Here, we denote the conventional cooperative NOMA as CC-NOMA. In this scheme, the system does not degenerate into the traditional NOMA transmission when $\rho = 0$.
- *CC-NOMA-STBC:* In this scheme, EH is not considered at the relay, i.e. $\rho$ in (9) is always zero.
- *EH IR C-NOMA:* Here IR denotes incremental relaying, which is similar to the solution proposed in this paper except that a single antenna, i.e. $L = 1$ is used at the source, relay and destination UE. This scheme is similar to the study presented in Liu *et al.* (2019).
- *EH C-NOMA w/o IR:* This scheme is also similar to the approach executed in EH CC-NOMA-STBC, except that each individual node in the network uses a single transmit antenna.

### 4.1 Outage probability of the destination user equipment

In Figure 2(a), we evaluate the OP performance of the destination UE according to equations (23) and (37) which are designated as proposed-exact and proposed-Asymp, respectively. Further, we set the target rate threshold for the relay and the destination UE to 1 bps/Hz. We observe that the analytical and the simulation results exhibit strong alignment, thus validating the accuracy of our analysis. Moreover, our proposed solution outperforms the benchmark schemes, EH CC-NOMA-STBC, CC-NOMA-STBC, EH IR C-NOMA, EH C-NOMA w/o IR by approximately 38%, 64%, 76% and 79%, respectively. The reasons for this are discussed as follows. In the case of EH CC-NOMA-STBC, only half of the entire time slot is always used when $\rho > 0$, unlike our proposed solution in which the system is enabled to degenerate into conventional NOMA where the entire time slot is used. In the CC-NOMA-STBC scheme, the relay is expected to always be in outage since EH is not considered. Thus, the OP in this scheme is only due to contributions from the source. Further, in the case of EH IR C-NOMA where $L = 1$, the OP is further degraded. Thus, this validates the fact that multiple antennas improve the diversity of the system, which in turn leads to a lower OP. The EH C-NOMA w/o IR scheme has the worst performance because the possibility of switching into conventional NOMA transmission is not considered.

In Figure 2(b), we study the OP behavior of the destination UE when $R_R > R_D$. A degradation in the outage performance of all the schemes is observed. For instance, in the low SNR region of approximately 4 dB, the outage probabilities of the proposed scheme in Figure 2(a) and Figure 2(b) are 0.3 and 0.6, respectively. In the high SNR region of approximately 23 dB, the corresponding outage probabilities are given as $1.6 \times 10^{-4}$ and $3.2 \times 10^{-3}$. To satisfy a higher rate threshold at the relay, the PS factor $\rho$ in (9), is further reduced to ensure the relay can successfully decode its information. However, this translates to a lower EH rate; consequently, the relay may be unable to forward the message to the destination UE. However, this challenge can be addressed by a careful selection of the PS factor.

### 4.2 Outage probability of the relay

In Figure 3(a), the OP of the relay is evaluated based on the expression in equation (55). We observe a higher OP at the relay compared with those obtained at the destination UE, as presented in Figure 2. For instance, in the proposed scheme under the equal rate threshold condition, the outage probabilities of the destination UE and the relay at an SNR of 20 dB are approximately $8.9 \times 10^{-4}$ and $1.2 \times 10^{-2}$, respectively. The key factors that could be responsible for this include the position of the relay from the source and the assigned power allocation and PS factors. Further, due to the incremental relaying strategy proposed, our scheme still outperforms other benchmark results. This is as a result of a lower minimum target rate required to satisfy the system outage constraints, i.e. $\psi' < \psi$, based on the expressions in equations (14) and (17). Therefore, to improve fairness in the system, a joint optimization of relay placement, PS and power allocation factors, should be incorporated. Further, in Figure 3(b), we study the effect of the higher rate threshold of the destination UE on the performance of the OP of the relay. When $R_D > R_R$, the relay could be unable to correctly decode the information of the destination device, which is also a condition for the relay to be in an outage, according to equation (54).

### 4.3 System throughput

Here, we examine the system throughput. First, we consider an equal target rate for the relay and the destination UE as depicted in Figure 4(a). The proposed method exhibits the overall best performance and improves with increasing SNR levels. However, the proposed solution and the baseline methods approach an upper bound throughput value in the high SNR region. In this region, the noise power is suppressed, and its effect on the received signal becomes negligible. However, this may increase the energy consumption in the network, consequently degrading the energy efficiency of the system. Thus, for optimal performance of the network, it is imperative that the design is made around the minimum SNR value of the convergence point, which in the considered scenario is approximately 30 dB. In Figure 4(b), we evaluate the performance of the system when $R_D > R_R$. As expected, a

**Figure 2** OP of the destination UE versus SNR

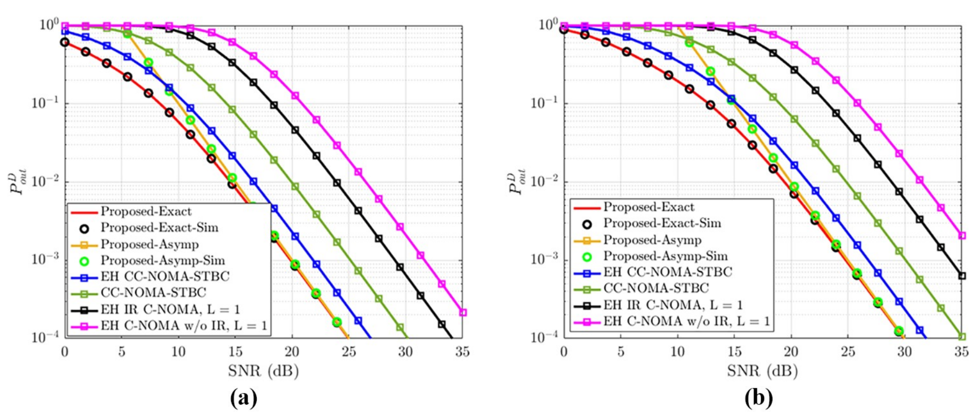


**Note(s):** (a) $R_D = R_R = 1$ bps/Hz; (b) $R_D = 2$ bps/Hz, $R_R = 1$ bps/Hz
**Source(s):** Authors' own work

World Journal of Engineering
Volume 23 · Number 2 · 2026 · 480–492

**Figure 3** OP of the relay versus SNR

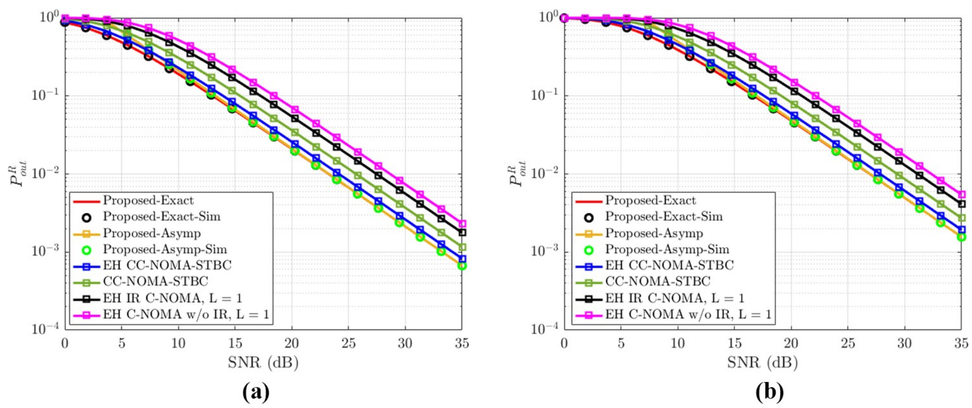


**Note(s):** (a) $R_D = R_R = 1$ bps/Hz; (b) $R_D = 2$ bps/Hz, $R_R = 1$ bps/Hz
**Source(s):** Authors' own work

**Figure 4** System throughput versus SNR

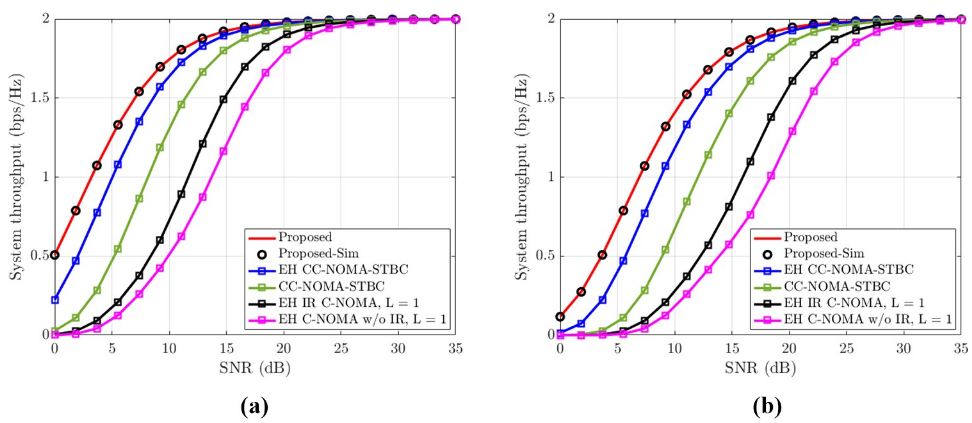


**Note(s):** (a) $R_D = R_R = 1$ bps/Hz; (b) $R_D = 2$ bps/Hz, $R_R = 1$ bps/Hz
**Source(s):** Authors' own work

lower system throughput is observed. However, our proposed method performs better than the benchmark schemes in the high SNR region.

### 4.4 *Energy efficiency* versus *transmit power*

Here, we examine the energy efficiency of the system as depicted in Figure 5(a). It is evident that for all the schemes, there is a decline in the energy efficiency of the system with an increase in transmit power. However, our solution still outperforms the benchmark schemes EH CC-NOMA-STBC, CC-NOMA-STBC, EH IR C-NOMA, EH C-NOMA w/o IR by approximately 44%, 60%, 75% and 83%, respectively. Aside from the diversity gain as a result of the STBC scheme, the incremental strategy proposed further improves the sum-rate of the system. Moreover, the harvested power $P_R$ in equation (9), used by the relay for transmission to the destination further contributed to the improved performance since it is recycled back into the system. Thus, the reason for assigning it a negative term in (58). Though it seems reasonable to increase the PS factor to achieve a higher harvested power at the relay, this may eventually impair the system energy efficiency. The reason is that an increase in PS factor will reduce the information decoding rate at the relay, consequently reducing its achievable rate. Further, we consider the scenario where the relay is deployed closer to the source as illustrated in Figure 5(b). At a transmit power of 10 dBm, an energy efficiency of $1.06 \times 10^4$ bits/joule is obtained in Figure 5(a), while a value $1.56 \times 10^4$ bits/joule is achieved in the case where the relay is positioned at 4 m away from the source. Hence, the source is able to reduce its transmit power due to the smaller distance between the source and the relay. Moreover, the results indicate that an optimal relay position exists and it should be deployed close to the source.

## 5. Conclusions

In this study, we have demonstrated the development and performance analysis of STBC-aided EH CNOMA. In the developed system, we incorporate the Alamouti STBC transmission scheme at the source and the relay nodes. In addition to the decode-and-forward protocol employed by the relay, a PS technique is also adopted to perform EH operations. Further, we enable the system to degenerate into traditional

**Figure 5** Energy efficiency versus transmit power

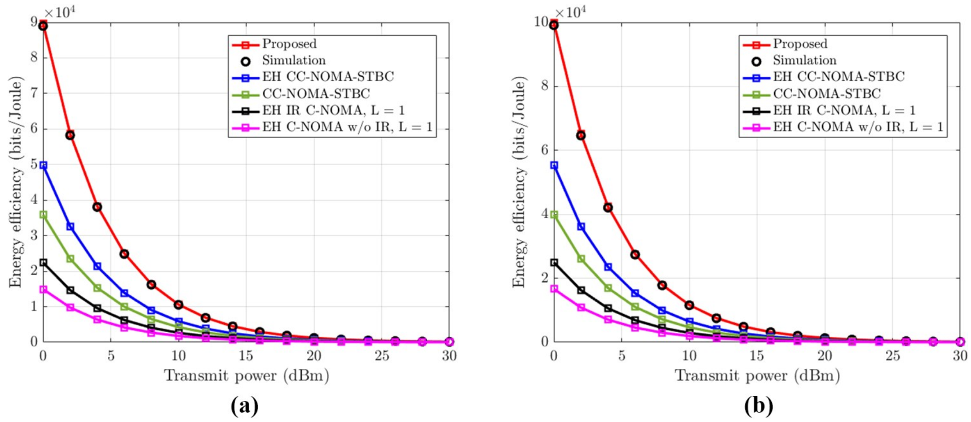


**Note(s):** (a) $d_1 = 10$ m, $d_2 = 4$ m; (b) $d_1 = 10$ m, $d_2 = 2$ m
**Source(s):** Authors' own work

NOMA transmission in a case where the relay is unable to perform EH operation. Based on this setup, we provide an extensive numerical analysis of the OP of the system. Furthermore, we examine the system throughput, energy efficiency and diversity order. Also, we compare our results with several benchmarks. These include non-degenerative STBC-aided cooperative NOMA with and without EH and single-antenna cooperative NOMA schemes. Our solution provides the optimal best performance in comparison to the benchmark scenarios. This study offers key insight into realizing the goals of 5G and beyond networks. These include an energy-efficient network design, seamless and massive connectivity of IoT devices, enhanced achievable data rate and throughput and sustainable network operation. In our future work, we shall broaden the analysis of this paper to capture more practical cases. This will involve the consideration of imperfect SIC and channel uncertainties in the system design.

## References

Agrawal, K., Jee, A. and Prakriya, S. (2024), "Performance of a multiuser cooperative IoT NOMA network with battery-assisted energy harvesting", *IEEE Transactions on Industrial Informatics*, Vol. 20 No. 2, pp. 2307-2319, doi: 10.1109/TII.2023.3290182.

Akhtar, M.W., Hassan, S.A., Saleem, S. and Jung, H. (2020), "STBC-Aided cooperative NOMA with timing offsets, imperfect successive interference cancellation, and imperfect channel state information", *IEEE Transactions on Vehicular Technology*, Vol. 69 No. 10, pp. 11712-11727, doi: 10.1109/TVT.2020.3017249.

Al Rabee, F.T., Masadeh, A., Abdel-Razeq, S. and Salameh, H.B. (2024), "Actor-Critic reinforcement learning for throughput-optimized power allocation in energy harvesting NOMA relay-assisted networks", *IEEE Open Journal of the Communications Society*, Vol. 5, pp. 7941-7953, doi: 10.1109/OJCOMS.2024.3514785.

Alamouti, S.M. (1998), "A simple transmit diversity technique for wireless communications", *IEEE Journal on Selected Areas in Communications*, Vol. 16 No. 8, pp. 1451-1458, doi: 10.1109/49.730453.

Alamu, O., Olwal, T.O. and Djouani, K. (2023a), "Cooperative NOMA networks with simultaneous wireless information and power transfer: an overview and outlook", *Alexandria Engineering Journal*, Vol. 71, pp. 413-438, doi: 10.1016/j.aej.2023.03.057.

Alamu, O., Olwal, T.O. and Djouani, K. (2023b), "An overview of simultaneous wireless information and power transfer in massive MIMO networks: a resource allocation perspective", *Physical Communication*, Vol. 57, p. 101983, doi: 10.1016/j.phycom.2022.101983.

Alamu, O., Olwal, T.O. and Djouani, K. (2023c), "Achievable rate optimization for space–time block code-aided cooperative NOMA with energy harvesting", *Engineering Science and Technology, An International Journal*, Vol. 40, p. 101365, doi: 10.1016/j.jestch.2023.101365.

Alamu, O., Olwal, T.O. and Djouani, K. (2024), "Sum-rate maximization for a distributed space-time block code-aided cooperative NOMA with energy harvesting", *Wireless Networks*, Springer, Cham, pp. 1-18, doi: 10.1007/s11276-024-03757-7.

Ashwini, K. and Jagadeesh, V.K. (2024), "Co-operative non-orthogonal multiple access networks: a survey", *World Journal of Engineering*, Vol. 21 No. 6, pp. 1128-1141, doi: 10.1108/WJE-11-2022-0451.

Bakshi, M., Lall, B., Mallik, R.K. and Singhal, A. (2024), "Performance of full-duplex cooperative NOMA network with direct link and battery-assisted non-linear energy harvesting near user", *IEEE Open Journal of the Communications Society*, Vol. Vol. 5, pp. 3484-3502, doi: 10.1109/OJCOMS.2024.3408313.

Björnson, E. and Demir, Ö.T. (2024), *Introduction to Multiple Antenna Communications and Reconfigurable Surfaces, Introduction to Multiple Antenna Communications and Reconfigurable Surfaces*, Now Publishers, MA, doi: 10.1561/9781638283157.

Demirkol, B., Toka, M. and Kucur, O. (2023), "Outage performance of NOMA with Alamouti/MRC in dual-hop

energy harvesting relay networks", *Physical Communication*, Vol. 58, p. 102026, doi: 10.1016/j.phycom.2023.102026.
Huang, H., Shi, Y., Liang, L., Zhang, X. and Wang, C. (2023), "On the outage probability of energy harvested cooperative multiuser cognitive NOMA network", *IET Communications*, Vol. 17 No. 13, pp. 1465-1477, doi: 10.1049/cmu2.12635.
Jorswieck, E.A. (2024), "Next-Generation multiple access: from basic principles to modern architectures", *Proceedings of the IEEE, Institute of Electrical and Electronics Engineers (IEEE)*, pp. 1-30, doi: 10.1109/jproc.2024.3412423.
Kader, M.F. and Shin, S.Y. (2017), "Cooperative relaying using space-time block coded non-orthogonal multiple access", ", *IEEE Transactions on Vehicular Technology*, Vol. 66 No. 7, pp. 5894-5903, doi: 10.1109/TVT.2016.2630706.
Khalaf, Q.M., Sali, A., Ismail, A., Ahmad, M.Y., Hussein, Y.S. and Shah, J.A. (2024), "Advanced nonlinear optimization techniques in SWIPT: a review", *IEEE Access*, Vol. 12, doi: 10.1109/ACCESS.2024.3519522.
Khennoufa, F., Khelil, A., Rabie, K., Kaya, H. and Li, X. (2023a), "An efficient hybrid energy harvesting protocol for cooperative NOMA systems: error and outage performance", *Physical Communication*, Vol. 58, p. 102061, doi: 10.1016/j.phycom.2023.102061.
Khennoufa, F., Khelil, A., Beddiaf, S., Kara, F., Rabie, K., Kaya, H., Emir, A., *et al.* (2023b), "Wireless powered cooperative communication network for Dual-Hop uplink NOMA with IQI and SIC imperfections", *IEEE Access*, Vol. 11, pp. 76506-76523, doi: 10.1109/ACCESS.2023.3297487.
Le, A.T., Tran, D.H., Le, C.B., Tin, P.T., Nguyen, T.N., Ding, Z., Poor, H.V., *et al.* (2024), "Power beacon and NOMA-assisted cooperative IoT networks with Co-Channel interference: performance analysis and deep learning evaluation", *IEEE Transactions on Mobile Computing*, Vol. 23 No. 6, pp. 7270-7283, doi: 10.1109/TMC.2023.3333764.
Li, E., Wang, Y., Liang, Z. and Zheng, M. (2023), "Improving the security and reliability of energy-constrained two-way relay systems with nonlinear energy harvesting", *IEEE Access*, Vol. 11, pp. 136793-136808, doi: 10.1109/ACCESS.2023.3339057.
Liu, C., Zhang, L., Chen, Z. and Li, S. (2023), "Power-time resource allocation for downlink SWIPT-assisted cooperative NOMA systems", *Science China Information Sciences*, Vol. 66 No. 5, p. 152303, doi: 10.1007/s11432-021-3495-y.
Liu, Y., Ding, H., Shen, J., Xiao, R. and Yang, H. (2019), "Outage performance analysis for SWIPT-based cooperative non-orthogonal multiple access systems", *IEEE Communications Letters*, Vol. 23 No. 9, pp. 1501-1505, doi: 10.1109/LCOMM.2019.2924655.
Moloudian, G., Hosseinifard, M., Kumar, S., Simorangkir, R.B.V.B., Buckley, J.L., Song, C., Fantoni, G., *et al.* (2024), "RF energy harvesting techniques for battery-less wireless sensing, industry 4.0, and internet of things: a review", *IEEE Sensors Journal*, Vol. 24 No. 5, pp. 5732-5745, doi: 10.1109/JSEN.2024.3352402.
Nagesham, G. and Vappangi, S. (2024), "Performance analysis of SWIPT NOMA with partial relay selection employing optimized power splitting factor", *IEEE Access*, Vol. 12, pp. 101419-101435, doi: 10.1109/ACCESS.2024.3431679.
Panse, V., Sharma, P.K., Jain, T.K. and Kothari, A. (2023), "Relay selection and nonlinear energy harvesting in full-duplex multi-relay cooperative network", *Physical Communication*, Vol. 56, p. 101946, doi: 10.1016/j.phycom.2022.101946.
Qian, L.P., Zhou, S., Wu, M. and Wu, Y. (2024), "Joint optimization of resource allocation and SIC ordering in energy-harvesting relay-aided NOMA NB-IoT networks", *IEEE Transactions on Green Communications and Networking*, Vol. 8 No. 1, pp. 468-481, doi: 10.1109/TGCN.2023.3330481.
Rahman, A.B. and Fazlul Kader, M. (2023), "A new energy harvesting scheme for multi-relay cooperative networks", *Digital Signal Processing*, Vol. 133, p. 103846, doi: 10.1016/j.dsp.2022.103846.
Ren, Y., Ren, B., Zhang, X., Lv, T., Ni, W. and Lu, G. (2023), "Impartial cooperation in SWIPT-Assisted NOMA systems with random user distribution", *IEEE Transactions on Vehicular Technology*, Vol. 72 No. 8, pp. 10488-10504, doi: 10.1109/TVT.2023.3261066.
Salim, M.M., Al-Dharrab, S.I., Costa, D.B. and Muqaibel, A.H. (2024), "Rate-Energy optimization for hybrid-powered full-duplex relays in cognitive C-NOMA with impairments", *IEEE Open Journal of the Communications Society*, Vol. 5, p. 7419-7433, doi: 10.1109/OJCOMS.2024.3500777.
Sharma, S., Mishra, A.K., Kumar, M.H., Deka, K. and Bhatia, V. (2024), "IRS-Enhanced cooperative NOMA: a contemporary review", *IEEE Access*.
Singh, S., Kumar, M. and Kumar, R. (2024), "Powering the future: a survey of ambient RF-based communication systems for next-gen wireless networks", *IET Wireless Sensor Systems*, doi: 10.1049/wss2.12094.
Sreenu, S. and Naidu, K. (2024), "Resource optimization for cooperative SWIPT-NOMA systems with imperfect SIC", *AEU - International Journal of Electronics and Communications*, Vol. 187, p. 155517, doi: 10.1016/j.aeue.2024.155517.
Tang, K., Xu, G., Yan, P., Zhu, H. and Feng, W. (2024), "Coverage performance of cooperative NOMA MmWave networks with wireless power transfer", *Computer Communications*, Vol. 218, pp. 85-96, doi: 10.1016/j.comcom.2024.01.008.
Tran, H.Q. and Vien, Q.-T.T. (2023), "SWIPT-Based cooperative NOMA for two-way relay communications: PSR versus TSR", *Wireless Communications and Mobile Computing*, Vol. 2023 No. 1, p. 3069999, doi: 10.1155/2023/3069999.
Ul Abidin Jaffri, Z. and Faheem, M. (2024), "Joint beamforming and power allocation design in cooperative MIMO-NOMA networks", *IEEE Access*, Vol. 12, pp. 114745-114759, doi: 10.1109/ACCESS.2024.3444696.
Wang, D., Gao, X. and You, X. (2006), "Low complexity turbo receiver for multi-user STBC block transmission systems", *IEEE Transactions on Wireless Communications*, Vol. 5 No. 10, pp. 2625-2632, doi: 10.1109/TWC.2006.04163.
Wei, Z., Xu, D., Li, S., Song, S., Ng, D.W.K. and Caire, G. (2024), "Resource allocation design for next-generation multiple access: a tutorial overview", *Proceedings of the IEEE, Institute of Electrical and Electronics Engineers (IEEE)*, pp. 1-34, doi: 10.1109/jproc.2024.3434700.
Xu, Z., Wang, S., Liu, D. and Wen, Z. (2021), "Joint beamforming and power-splitting optimization for SWIPT-enabled MISO full-duplex two-way cooperative NOMA systems", *Physical Communication*, Vol. 45, p. 101257, doi: 10.1016/j.phycom.2020.101257.
Xu, X., Liu, Y., Mu, X., Chen, Q. and Ding, Z. (2023), "Cluster-free NOMA communications toward next

generation multiple access", *IEEE Transactions on Communications*, Vol. 71 No. 4, pp. 2184-2200, doi: 10.1109/TCOMM.2023.3244926.

Yang, Z., Xia, L., Cui, J., Dong, Z. and Ding, Z. (2024), "Delay and energy minimization for cooperative NOMA-MEC networks with SWIPT aided by RIS", *IEEE Transactions on Vehicular Technology*, Vol. 73 No. 4, pp. 5321-5334, doi: 10.1109/TVT.2023.3332729.

Yuan, Y., Xu, Y., Yang, Z., Xu, P. and Ding, Z. (2019), "Energy efficiency optimization in full-duplex user-aided cooperative SWIPT NOMA systems", *IEEE Transactions on Communications*, Vol. 67 No. 8, pp. 5753-5767, doi: 10.1109/tcomm.2019.2914386.

Zeng, M., Hao, W., Dobre, O.A. and Ding, Z. (2020), "Cooperative NOMA: state of the art, key techniques, and open challenges", *IEEE Network*, Vol. 34 No. 5, pp. 205-211, doi: 10.1109/MNET.011.1900601.

Zhai, C., Li, Y., Wang, X., Zheng, L. and Li, C. (2024a), "Wireless powered cooperative NOMA with Alamouti coding and selection relaying", *IEEE Transactions on Mobile Computing*, Vol. 23 No. 2, pp. 1366-1381, doi: 10.1109/TMC.2023.3235394.

Zhai, C., Yu, J., Du, K., Dai, H., Wang, X. and Li, Y. (2024b), "Nonlinear energy harvesting based alternate cooperative nonorthogonal multiple access with adaptive interference cancellation", *Computer Networks*, Vol. 240, p. 110169, doi: 10.1016/j.comnet.2024.110169.

Zwillinger, D. and Jeffrey, A. (2000), *Table of Integrals, Series, and Products*, Academic press.

## About the authors

**Olumide Alamu** received the BTech degree in Electronic and Electrical Engineering from Ladoke Akintola University of Technology, Nigeria, in 2009, MSc degree in Electrical and Electronics Engineering from the University of Lagos, Nigeria, in 2016, and DEng degree in Electrical Engineering from the Tshwane University of Technology (TUT), South Africa, in 2024. He is currently on a postdoctoral fellowship programme at the Department of Electrical Engineering/F'SATI, TUT. His current research interests include wireless communication systems modeling and optimization, Machine learning applications in wireless communication systems, and green wireless communications. Olumide Alamu is the corresponding author and can be contacted at: alamuoa@tut.ac.za

**Thomas O. Olwal** received PhD degree in Computer Science from the University of Paris-EST, Champs-sur-Marne, France, in 2011, and the DTech degree in Electrical Engineering from Tshwane University of Technology (TUT) (in a cotutelle programme), Pretoria, South Africa, in 2011. He is a senior member of the IEEE and works as a Professor with the Department of Electrical Engineering at TUT. His research interests include analysis and design of the 5G and beyond networks, efficient spectrum and energy resource management, wireless sensor networks, Internet of Things, ubiquitous and green computing for sustainable development. He has served as a TCP member in a number of IEEE conferences and a reviewer in ISI/Scopus-indexed journals.

**Munguakonkwa Emmanuel Migabo** received the DEng degree in Electrical Engineering from the Tshwane University of Technology, Pretoria, South Africa, in 2021, and a PhD in Computer Science from the University of Paris Est in France. He is currently a senior lecturer and researcher within the Department of Electrical Engineering at the Tshwane University of Technology. His current research interests include energy-efficient channel coding techniques, data rate enhanced modulation scheme techniques, and link adaptation schemes for enhanced scalability, all for the Narrowband Internet of Things. He has previously worked on energy-efficient, scalable and balanced routing and network coding techniques for wireless sensor networks on which he has published several conference and journal articles.